J. Fluid Mech. (1983), *vol.* 126, *pp.* 75–89
Printed in Great Britain

Three-dimensional simulations of convection in layers with tilted rotation vectors

By DAVID H. HATHAWAY†

Advanced Study Program and High Altitude Observatory, National Center for Atmospheric Research, Boulder, CO 80307, U.S.A.

AND RICHARD C. J. SOMERVILLE

Scripps Institution of Oceanography, University of California, San Diego, La Jolla, CA 92093, U.S.A.

(Received 18 November 1981 and in revised form 18 February 1982)

Three-dimensional and time-dependent numerical simulations of thermal convection are carried out for rotating layers in which the rotation vector is tilted from the vertical to represent various latitudes. The vertical component of the rotation vector produces narrow convection cells and a reduced heat flux. As this vertical component of the rotation vector diminishes in the lower latitudes, the vertical heat flux increases. The horizontal component of the rotation vector produces striking changes in the convective motions. It elongates the convection cells in a north–south direction. It also tends to turn upward motions to the west and downward motions to the east in a manner that produces a large-scale circulation. This circulation is directed to the west and towards the poles in the upper half of the layer and to the east and towards the equator in the bottom half. Since the layer is warmer on the bottom this circulation also carries an equatorward flux of heat. When the rotation vector is tilted from the vertical, angular momentum is always transported downwards and toward the equator. For rapidly rotating layers, the pressure field changes in a manner that tends to balance the Coriolis force on vertical motions. This results in an increase in the vertical heat flux as the rotation rate increases through a limited range of rotation rates.

1. Introduction

In many geophysical and astrophysical fluid systems the circulations are dominated by the profound influence of rotation upon one form or another of thermal convection. For this reason the study of idealized types of convection with rotation has provided many fruitful insights into the dynamics of such complicated and disparate fluids as stellar and planetary atmospheres. Many properties of the general circulation of the earth's atmosphere, for example, have been illuminated by the study of thermal convection in a rotating cylindrical annulus with an imposed horizontal temperature gradient. Dramatically different circulation patterns are found in different regions of parameter space for this relatively simple system. This fact provided one of the earliest and clearest demonstrations that the nature of the general circulation cannot be inferred from purely qualitative reasoning but instead depends strongly on the quantitative specifications of the system (cf. Lorenz 1967).

The classical Rayleigh–Bénard convection problem, in which the flow is driven by

† Present address: Sacramento Peak Observatory, Sunspot, NM 88349, U.S.A.

an imposed vertical temperature gradient, has provided the basis for many studies of convection with rotation. Among the earliest theoretical investigations were linear stability analyses in which the horizontally unbounded plane parallel geometry of the classical problem was retained. Uniform rotation about a vertical axis was the only added ingredient (cf. Veronis 1959; Chandrasekhar 1961; Weiss 1964; Heard & Veronis 1971). Subsequent linear stability theories were carried out for the onset of convection in rotating spheres (Roberts 1968; Busse 1970*a*) and rotating spherical shells with radial temperature gradients (Busse 1970*b*; Heard 1972; Gilman 1975; Busse & Cuong 1977).

Recently, linear stability analyses have been presented for plane parallel fluid layers in which the temperature gradient and rotation vector need not be parallel to gravity (Flasar & Gierasch 1978; Hathaway, Gilman & Toomre 1979; Hathaway, Toomre & Gilman 1980). These analyses have been one of the primary motivations for our nonlinear numerical simulations. They suggest that a tilted rotation vector may give rise to a rich variety of convective structures. Among natural systems, the striking features of the atmospheric circulation of Jupiter and the solar differential rotation are among the most prominent examples of phenomena which may, at least in part, be understood in terms of the latitude-dependent effects of rotation on thermal convection.

The finite-amplitude properties of convection with a vertical imposed temperature gradient and a vertical rotation vector have been explored in laboratory experiments (Koschmieder 1967; Rossby 1969; Krishnamurti 1971) and in nonlinear numerical simulations. Veronis (1968) and Somerville (1971) carried out two-dimensional numerical simulations, while Clever & Busse (1979) and Busse & Heikes (1980) have explored the stability of the finite-amplitude solutions, a subject pioneered by Kuppers & Lortz (1969) and Kuppers (1970). Three-dimensional numerical simulations have been reported by Somerville & Lipps (1973) and nonlinear solutions of single-mode equations have been studied by Van der Borght & Murphy (1973) and by Baker & Spiegel (1975).

The effects of a tilted rotation vector are difficult to explore in laboratory experiments, and so the role of numerical simulation in this case is an especially important one. Fortunately, recent developments in numerical methods, together with advances in computer power, have made fully three-dimensional and time-dependent simulations of thermal convection much more feasible than was the case only a few years ago. We have taken advantage of this technological progress to carry out exploratory simulations of several cases of convection in which the imposed temperature gradient is parallel to gravity but the rotation vector need not be. The numerical procedure we use is an efficient implicit finite-difference technique described by Somerville & Gal-Chen (1979). Used on the Cray-1 computer at the National Center for Atmospheric Research (NCAR), this method typically requires about $\frac{1}{2}$ h of computer time to simulate the evolution of one case to a quasi-equilibrium state. We have found that computer-generated motion pictures are a virtually indispensable aid to the analysis of our four-dimensional numerical solutions. The availability at NCAR of the necessary machinery, software, and expertise in computer graphics has been part of the technological resources that have made our research possible.

In this study we have carried out four numerical integrations in which the effects of varying the rotation vector are illustrated. Although our four cases are by no means an adequate exploration of parameter space, they do provide an intriguing sample of the multiplicity of the possible modes of convection. Our results answer some questions, raise others, and suggest several extensions and applications for future study. One application, to solar rotation effects in supergranules, has already been

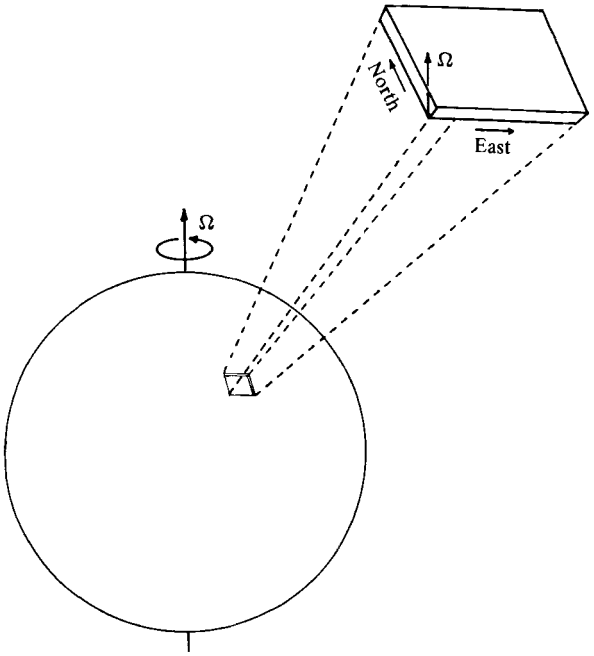

FIGURE 1. The geometry used in the model. A plane parallel layer of fluid is positioned tangent to a sphere at some latitude φ. The rotation vector is then tilted from the vertical with a northward component as well as a vertical component.

investigated (Hathaway 1982). We have chosen a highly idealized system for study and have modelled it using the Bousinesq equations. Our representation of the influence of rotation is quite general, in that we have retained all of the Coriolis terms rather than making any *a priori* assumptions concerning their relative magnitudes. Thus we have approached the problem as one in pure fluid dynamics, but we expect our results to be applicable to understanding convection with rotation in a wide variety of stellar and planetary contexts.

2. The model

We use a three-dimensional and time-dependent numerical model to simulate the convective flow within a rotating plane parallel layer. The geometry employed is shown in figure 1. The layer of fluid is positioned tangent to the sphere at some latitude φ. We neglect the effects of curvature but include both the vertical and the horizontal components of the rotation vector to simulate various latitudes. The Cartesian coordinate system we use has x increasing towards the east, y increasing towards the north, and z increasing upwards, antiparallel to gravity. We employ the Boussinesq approximation, in which the fluid is assumed to be of constant density except for small variations (due to temperature), which couple with gravity to produce the buoyant force that drives the motions.

A grid-point model is used to represent the fluid velocity, temperature and pressure at discrete time and space intervals. The diffusivities κ and ν of heat and momentum are taken to be constants that are independent of position or temperature. The full set of equations are then the equation of mass continuity

$$\frac{\partial u}{\partial x}+\frac{\partial v}{\partial y}+\frac{\partial w}{\partial z}=0, \tag{2.1}$$

the three components of the momentum equation

$$\frac{\partial u}{\partial t}+u\frac{\partial u}{\partial x}+v\frac{\partial u}{\partial y}+w\frac{\partial u}{\partial z}-2\Omega\sin\phi v+2\Omega\cos\phi w=-\frac{1}{\rho}\frac{\partial p}{\partial x}+\nu\nabla^2 u, \tag{2.2}$$

$$\frac{\partial v}{\partial t}+u\frac{\partial v}{\partial x}+v\frac{\partial v}{\partial y}+w\frac{\partial v}{\partial z}+2\Omega\sin\phi u=-\frac{1}{\rho}\frac{\partial p}{\partial y}+\nu\nabla^2 v, \tag{2.3}$$

$$\frac{\partial w}{\partial t}+u\frac{\partial w}{\partial x}+v\frac{\partial w}{\partial y}+w\frac{\partial w}{\partial z}-2\Omega\cos\phi u=-\frac{1}{\rho}\frac{\partial p}{\partial z}-(1-\alpha T)g+\nu\nabla^2 w, \tag{2.4}$$

and the heat equation

$$\frac{\partial T}{\partial t}+u\frac{\partial T}{\partial x}+v\frac{\partial T}{\partial y}+w\frac{\partial T}{\partial z}=\kappa\nabla^2 T, \tag{2.5}$$

where (u, v, w) is the fluid velocity in the (x, y, z)-direction, p is the pressure, T is the temperature, ρ is the fluid density, Ω is the rotation frequency, α is the volumetric coefficient of thermal expansion and g is the gravitational acceleration.

It is useful to rewrite these equations in a dimensionless form with the basic background distributions of pressure, temperature, and density removed. On taking the depth D of the layer as the unit of length, the viscous diffusion time D^2/ν as the unit of time, and the temperature difference ΔT across the layer as the unit of temperature, (2.1)–(2.5) become

$$\frac{\partial u}{\partial x}+\frac{\partial v}{\partial y}+\frac{\partial w}{\partial z}=0, \tag{2.6}$$

$$\frac{\partial u}{\partial t}+u\frac{\partial u}{\partial x}+v\frac{\partial u}{\partial y}+w\frac{\partial u}{\partial z}-Ta^{\frac{1}{2}}\sin\phi v+Ta^{\frac{1}{2}}\cos\phi w=-\frac{\partial p}{\partial x}+\nabla^2 u, \tag{2.7}$$

$$\frac{\partial v}{\partial t}+u\frac{\partial v}{\partial x}+v\frac{\partial v}{\partial y}+w\frac{\partial v}{\partial z}+Ta^{\frac{1}{2}}\sin\phi u=-\frac{\partial p}{\partial y}+\nabla^2 v, \tag{2.8}$$

$$\frac{\partial w}{\partial t}+u\frac{\partial w}{\partial x}+v\frac{\partial w}{\partial y}+w\frac{\partial w}{\partial z}-Ta^{\frac{1}{2}}\cos\phi u=-\frac{\partial p}{\partial z}+\frac{Ra}{Pr}T+\nabla^2 w, \tag{2.9}$$

$$\frac{\partial T}{\partial t}+u\frac{\partial T}{\partial x}+v\frac{\partial T}{\partial y}+w\frac{\partial T}{\partial z}=\frac{1}{Pr}\nabla^2 T, \tag{2.10}$$

where

$$Ta=\frac{4\Omega^2 D^4}{\nu^2} \tag{2.11}$$

is the Taylor number,

$$Ra=\frac{\alpha g\Delta T D^3}{\kappa\nu} \tag{2.12}$$

is the Rayleigh number, and

$$Pr=\frac{\nu}{\kappa} \tag{2.13}$$

is the Prandtl number.

These equations (2.6)–(2.10) are marched forward in time using an extension of a method first suggested by Chorin (1968) and described in more detail by Somerville & Gal-Chen (1979). The time differencing is implicit, to allow larger time steps, and the pressure is calculated using an iterative technique. We use rigid (non-slip) top and bottom boundaries and periodic side boundaries to represent an infinite plane parallel layer. The computational domain measures 1 unit in the z-direction by 6·0 units in the x-direction by 4·9 units in the y-direction, and involves 38400 grid points in an array with 48 points in x, 32 points in y, and 25 points in z. One time step takes 2–4 s on the CRAY-1 computer at NCAR, depending upon how many iterations are required to obtain the pressure.

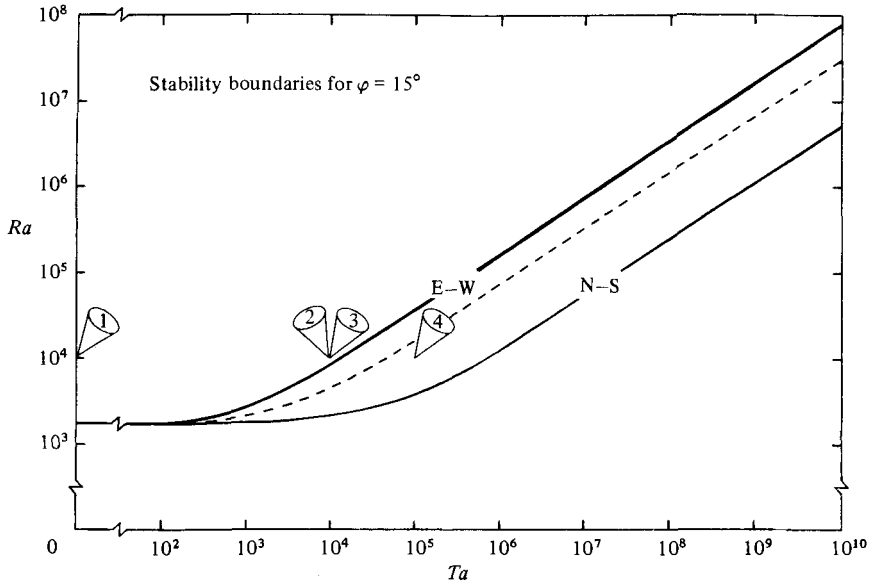

FIGURE 2. The stability boundaries for convective rolls at 15° latitude. The layer is unstable for Rayleigh numbers above these curves. Rolls oriented east–west (E–W) require larger Rayleigh numbers than do north–south (N–S) rolls. The dashed line represents the stability boundary for convective rolls at 90° latitude. The numbered points refer to the cases described in the text.

We integrated four cases for this study. The Prandtl number was taken to be unity in all of them since the computer code runs most efficiently for this value. We also set $Ra = 10^4$ in all four runs so that the thermal forcing remained the same, thereby allowing a straightforward analysis of the effects of rotation and the tilted rotation vector.

For the first run we set $Ta = 0$ to provide a non-rotating reference state with which the rotating cases could be compared. This calculation was started from a static state in which small temperature perturbations were superimposed on a horizontally uniform temperature field that decreased linearly with height. Each of the following three cases used the end of the previous case for its initial condition. In the second run we took $Ta = 10^4$ and $\varphi = 90°$ to give a moderately rotating case with a vertical rotation vector. For the third case we again took $Ta = 10^4$, but tilted the rotation vector to represent a low latitude with $\varphi = 15°$. For the fourth case we increased Ta to 10^5 while keeping $\varphi = 15°$. This produced a rapidly rotating case in which the effects of rotation dominate the flow.

The parameter values associated with these four cases are represented by the numbered points in figure 2. In this figure the stability boundaries for roll-like disturbances oriented north–south (N–S) or east–west (E–W) at a latitude of 15° are represented by the solid lines. The stability boundary for 90° latitude is represented by the dashed line. The location of these boundaries was determined using a linear stability analysis like that described in Hathaway *et al.* (1980). For parameter values above these lines the layers are unstable, and convective motions will carry much of the heat flux. At 90° latitude there is no unique horizontal direction, so a single curve represents all possible orientations for convective rolls. At 15° the horizontal component of the rotation vector provides a unique direction, and a number of stability boundaries can be drawn depending upon the roll orientation. The separation of the curves in figure 2 shows that rolls oriented north–south are unstable for much

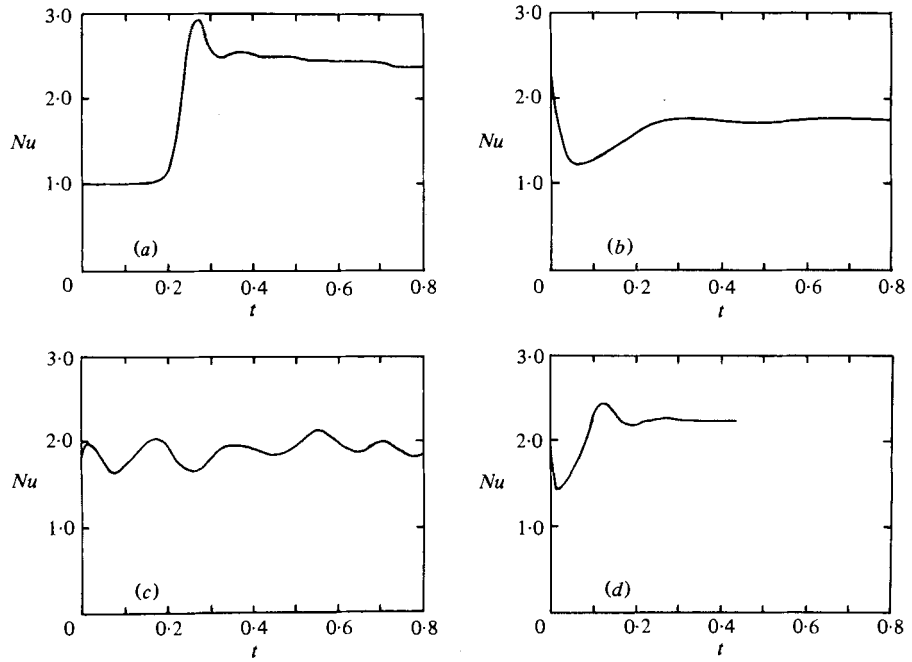

FIGURE 3. The Nusselt numbers Nu plotted as functions of time t for the four cases studied.

smaller temperature gradients than those required to make the east–west rolls unstable. All convective roll orientations are unstable for the first three cases, but the rolls oriented east–west are stable in the fourth case. In §3 we will analyse the resulting motions for these four cases to determine the effects of the tilted rotation vector on the flow.

3. The results

The transport properties of the convective motions are of major importance for many geophysical and astrophysical systems. The rate at which heat can be transported across the layer determines the vertical stratification while a horizontal heat transport can limit or induce horizontal variations in the temperature field. Vertical and horizontal transports of momentum can also be produced and these transports can induce large-scale flows that influence the basic structure of the system. In this section we analyse the velocity, temperature and pressure fields to determine these transport properties and how they depend upon the tilted rotation vector.

3.1. *Heat flux*

A variety of measures can be used to characterize the convective flows. One of the most important of these is the heat flux that is transported across the layer. In dimensionless units this flux is given by the Nusselt number

$$Nu = 1 + \langle wT \rangle, \tag{3.1}$$

which is the ratio of the total heat flux to that which would be carried by conduction alone (here the angle brackets represent a volume average). The Nusselt numbers for the four cases studied here are plotted in figure 3 as functions of time.

The heat flux for the first case is shown in figure 3(*a*). Since this case was started from small random temperature perturbations there is a rather lengthy initial period

during which the fluid is almost motionless. At about $t = 0{\cdot}2$ the most unstable mode of convection becomes energetic enough to become noticeable. The initial exponential rise is damped out as changes appear in the background temperature distribution and in the form of the convection itself. The heat flux then asymptotes at a Nusselt number of about 2·4 and a dimensionless r.m.s. fluid velocity of about 17.

The time dependence of the heat flux for the second case is shown in figure 3(*b*). After an initial rapid decay the flux rises slowly to a fairly steady level with $Nu = 1{\cdot}75$. The cinematic animation of the flow shows that the initial decay is due to the damping of the rather large convective cells initially present from the previous run. As these modes decay new ones grow that have smaller horizontal dimensions. Typical fluid velocities are about 10 and they carry a correspondingly smaller heat flux.

The heat flux for the third case is shown in figure 3(*c*). In this case the flux oscillates while rising slightly to a value of about 2·0. Fluid velocities of about 14 give turnover times that are comparable to the rotation period, and both timescales are similar to the period of the heat-flux oscillations. This coincidence tends to make the source of these oscillations uncertain. Since the rotation rate for this case is the same as for the second case, the larger heat flux must be associated with the tilt of the rotation vector. The linear stability analyses show in fact that only the vertical component of the rotation vector figures in the stability analysis for convective rolls oriented north–south. Thus this low-latitude case is more unstable and consequently gives larger velocities and heat flux.

The time history of the heat flux for the fourth case is shown in figure 3(*d*). After an initial drop like that in the second case the heat flux rises again and becomes almost steady with $Nu = 2{\cdot}2$. In spite of the more rapid rotation rate this flux exceeds that obtained in the third case and approaches the value of the heat flux for the non-rotating case. Typical fluid velocities are about 15 for this case. The reason for this increased heat flux is due to the adjustments in the velocity field caused by rotation and will be discussed in §3.2.

Horizontal heat fluxes are produced in the third and fourth cases even though large-scale horizontal temperature gradients are absent. A heat flux in the east–west direction returns on itself and can have no divergence and cannot therefore introduce any heating or cooling to different parts of the system. A north–south heat flux can, and in fact must, vary with latitude, and is thereby capable of heating or cooling different latitude bands. We find that an equatorward flux of heat is produced in both the third and fourth cases. For the third case this flux is about 18% of the total vertical heat flux while the flux in the fourth case is only about 3% of the vertical flux. This latitudinal flux must vanish at the poles due to a lack of any preferred direction there. It must also vanish at the equator since we expect the flows to be symmetric about the equator. Thus this equatorward heat flux must product a net heating of the equatorial regions and a cooling of the polar regions. The means by which this heat flux is produced will be discussed in §3.3.

3.2. *Flow structure*

The cinematic animation of the velocity and temperature fields was instrumental in understanding the evolution of the flow patterns. For the first case the fluid remains static until $t = 0{\cdot}2$, at which time the motions are discernible and rapidly accelerating. The horizontal scale of the motions at this time is comparable to the depth of the layer and agrees fairly well with the wavelength of the most unstable mode from linear theory. As the flow evolves adjacent cells coalesce to form larger ones until the flow becomes fairly steady with two major cells within the computational domain.

The flow within these cells is fairly isotropic with nearly equal amounts of kinetic energy in the vertical and horizontal directions. This is in contrast to the most unstable mode from linear theory which has more kinetic energy in the vertical direction.

The final flow field for this first case is shown in figure 4 (plate 1). Here a three-dimensional perspective view of particle trajectories is shown. The overturning motions can be seen in the two vertical planes. On the horizontal upper surface the particles spread out from the updrafts (vacant regions) and converge on the downdrafts (filled regions). The horizontal size of these convective elements is considerably larger than that given by the most unstable mode. The cells may in fact be too large in that the size of the computational domain may very well limit any further evolution. We chose not to increase the size of the domain, however, because the smaller cells expected in later calculations would then be poorly resolved.

The final flow field for the second case is shown in figure 5 (plate 1) using the same perspective view used in figure 4. The smaller size of the convective elements is immediately evident as is the turning effect of the Coriolis forces. On the horizontal surface the outflows from the updraft are turned clockwise (anticyclonically) while the convergent flows near the downdrafts are turned counterclockwise (cyclonically). This sense of turning switches near the bottom of the layer, as was pointed out by Veronis (1959), thereby giving a twisting motion to fluid columns. Since these curved trajectories and small cell sizes are more susceptible to dissipative effects the resultant motions are much slower. The narrow cells and moderate twisting due to Coriolis forces produce an anisotropic flow field with more kinetic energy in the vertical direction.

When the rotation vector is tilted from the vertical in the third case the flow field changes considerably. The final flow field for this case is shown in figure 6 (plate 2). Here the tilted rotation vector plays an important role. The convective elements tend to be elongated in a north–south direction as shown by the fairly prominent rows of convergent and divergent flows. There is also a strong correlation between upward motions and westward motions. This correlation is evident in the trajectories plotted on the southern vertical plane and is measured to be

$$\frac{\langle uw \rangle}{(\langle u^2 \rangle \langle w^2 \rangle)^{\frac{1}{2}}} = -0{\cdot}3. \tag{3.2}$$

The source of these tilted trajectories is easily attributed to the presence of the horizontal component of the rotation vector. Upward-moving elements tend to conserve their angular momentum and move toward the west under the influence of the Coriolis forces. This general behaviour is also predicted by linear theory.

Figure 7 (plate 2) shows the particle trajectories for the fourth case. Here the rapid rotation of the layer produces a regular array of convective rolls with north–south axes. Although the Coriolis forces are much stronger here than in the third case the tilting of the vertical flow is no longer evident. We find in fact that

$$\frac{\langle uw \rangle}{(\langle u^2 \rangle \langle w^2 \rangle)^{\frac{1}{2}}} = -0{\cdot}015, \tag{3.3}$$

which implies that the fluid moves nearly vertically upward. This explains the larger heat flux for this case. By moving vertically upward, instead of at some angle as in the third case, the motions are more efficient in transporting heat across the layer. These vertically moving fluid elements do not conserve their angular momentum. Cowling (1951) shows that non-conservation of angular momentum by fluid parcels

could occur for non-axisymmetric modes. For such modes of convection the pressure field shifts to balance the Coriolis forces due to the horizontal component of the rotation vector.

Although, in this case, the Coriolis forces due to the horizontal component of Ω are largely balanced by pressure gradients, those forces due to the vertical component of Ω are unbalanced, as is seen in the flow field in the horizontal plane. Here fluid elements are turned to the right as they move from updraughts to downdraughts, so that fluid moving eastward from an updraught gets turned to the south. This effect is particularly evident here because of the regularity of the convection rolls. We find

$$\frac{\langle uv \rangle}{(\langle u^2 \rangle \langle v^2 \rangle)^{\frac{1}{2}}} = -0{\cdot}80 \tag{3.4}$$

for this case, while for the third case we find

$$\frac{\langle uv \rangle}{(\langle u^2 \rangle \langle v^2 \rangle)^{\frac{1}{2}}} = -0{\cdot}16. \tag{3.5}$$

The larger value of this correlation for case 4 is due to the combined effects of the vertical component of Ω turning the horizontal velocities and the horizontal component of Ω producing a series of north–south rolls instead of horizontally isotropic cells.

3.3. *Mean flows*

The tilted rotation vector can induce mean flows by producing correlations between the various velocity components. These velocity correlations can be thought of as momentum fluxes with $\langle uw \rangle$ and $\langle uv \rangle$ the vertical and latitudinal fluxes of zonal (eastward) momentum, and $\langle vw \rangle$ the vertical flux of latitudinal (northward) momentum. A convergence of these fluxes in any region will then deposit momentum there in a manner that produces a mean flow.

The source of any mean flow can be determined by taking the horizontal average of the momentum equations (2.7) and (2.8), which gives

$$\frac{\partial \bar{u}}{\partial t} = -\frac{\partial}{\partial z}\overline{uw} + Ta^{\frac{1}{2}} \sin\phi \bar{v} + \frac{\partial^2 \bar{u}}{\partial z^2}, \tag{3.6}$$

$$\frac{\partial \bar{v}}{\partial t} = -\frac{\partial}{\partial z}\overline{vw} - Ta^{\frac{1}{2}} \sin\phi \bar{u} + \frac{\partial^2 \bar{v}}{\partial z^2}, \tag{3.7}$$

where the overbar represents horizontally averaged quantities. The first term on the right-hand side of these equations represents the divergence of the vertical flux of zonal and latitudinal momentum. Since $\langle uw \rangle$ is negative for these cases and must vanish at the top and bottom boundaries, there must be a divergence of zonal momentum from the upper regions of the layer and a convergence in the lower regions. We also find that $\langle vw \rangle$ is negative in the third and fourth cases, with

$$\frac{\langle vw \rangle}{(\langle v^2 \rangle \langle w^2 \rangle)^{\frac{1}{2}}} = -0{\cdot}13 \tag{3.8}$$

in case 3, and

$$\frac{\langle vw \rangle}{(\langle v^2 \rangle \langle w^2 \rangle)^{\frac{1}{2}}} = -0{\cdot}05 \tag{3.9}$$

in case 4. Thus latitudinal momentum is also extracted from the upper region and deposited in the lower region.

While the divergence of these momentum fluxes provides the initial driving for the

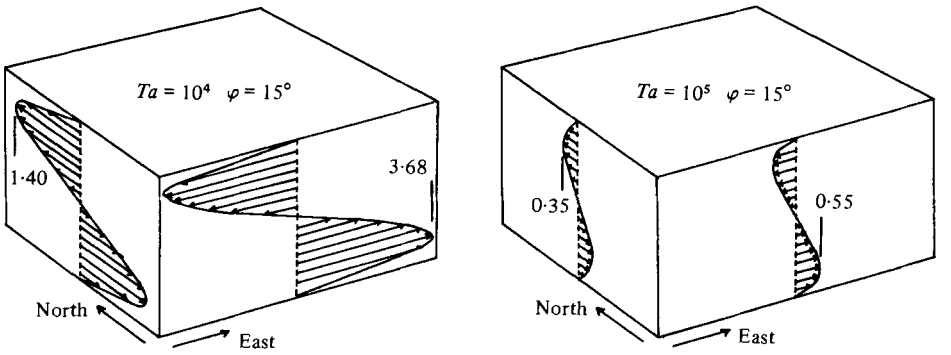

FIGURE 8. The mean flows produced in cases 3 and 4. The induced flow is to the west and north in the upper half of the layer and to the east and south in the lower half. These flows are much weaker in the rapidly rotating case because the pressure field balances the Coriolis forces to produce weak momentum fluxes.

mean flows, the Coriolis forces will come into play once the mean flows are established. These forces are represented by the second term on the right-hand sides of (3.6) and (3.7). The momentum fluxes for these cases tend to produce a flow that is to the east and north along the bottom and to the west and south along the top. The Coriolis force on the northward and southward flows tends to reinforce the east–west flows. However, the Coriolis force in (3.7) on the eastward and westward flows tends to oppose the north–south flows. The final term on the right-hand sides of (3.6) and (3.7) represents the viscous diffusion of the mean flow, and as such limits the amplitude of the resultant flows.

The final mean flows produced in the third and fourth cases are shown in figure 8. As expected, the flow is to the west along the top and to the east along the bottom. The north–south flow, however, is dominated by the effect of the Coriolis forces on the zonal flow, which produces a northward flow along the top and a southward flow along the bottom.

These mean flows drive the latitudinal heat flux. This flux is given by the correlation of latitudinal flows with temperature. While the convective motions can produce correlations between v and the temperature perturbations we find that the primary source of the equatorward heat flux is the advection of the mean temperature field by the mean flow. Since the layer is warmer on the bottom the equatorward flow there carries heat toward the equator.

Since the momentum fluxes are weaker in case 4 the resultant mean flow is slower than that produced in case 3. The source of the smaller values of $\langle uw \rangle$ in the fourth case can be seen in the pressure field. An equation for the pressure can be formed by taking the divergence of the momentum equations (2.7)–(2.9). This gives

$$\nabla^2 p = \frac{Ra}{Pr}\frac{\partial T}{\partial z} + Ta^{\frac{1}{2}} \sin\phi\, \zeta + Ta^{\frac{1}{2}} \cos\phi\, \eta + \mathrm{NL}, \tag{3.10}$$

where

$$\zeta = \frac{\partial v}{\partial x} - \frac{\partial u}{\partial y} \tag{3.11}$$

is the vertical vorticity,

$$\eta = \frac{\partial u}{\partial z} - \frac{\partial w}{\partial x} \tag{3.12}$$

is the northward vorticity, and NL represents the nonlinear terms. The first term on the right-hand side of (3.10) represents the hydrostatic contribution to the pressure

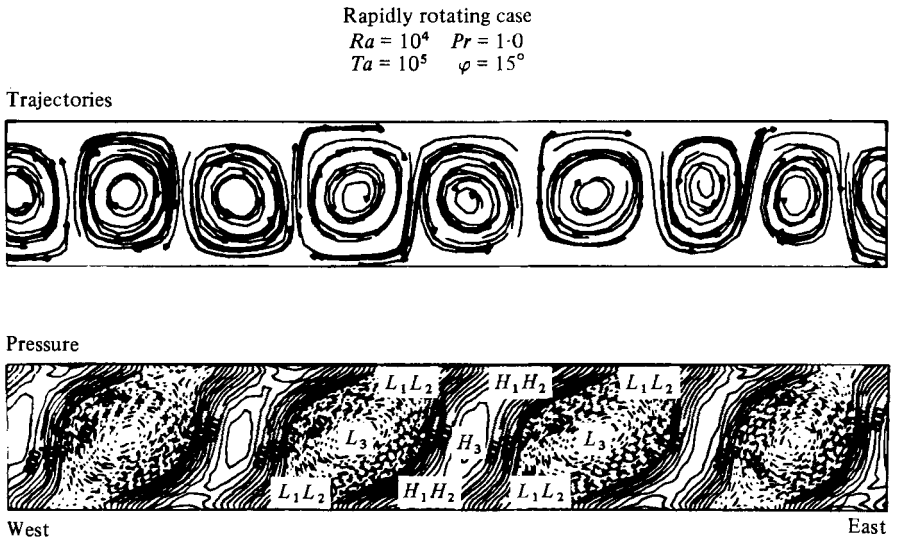

FIGURE 9. Trajectories and pressure contours for case 4. Here the pressure contribution (H_3, L_3) due to the horizontal component of the rotation vector dominates the contributions due to hydrostatics (H_1, L_1) and the vertical component of the rotation vector (H_2, L_2). The resulting pressure gradients balance the Coriolis forces on the vertical flows to produce upward motions which are nearly vertical.

from temperature-produced density variations. This term produces the high-pressure regions at the top of updraughts and at the bottom of downdraughts. These high-pressure regions drive the horizontally divergent flows near the top and bottom, while the low-pressure regions drive the horizontally convergent flows. The second term on the right-hand side of (3.10) represents a contribution due to the vertical component of $\boldsymbol{\Omega}$. This term tends to enhance the hydrostatic contribution by producing high pressure in the horizontally divergent regions where the vertical vorticity is negative (anticyclonic) and low pressure in the convergent regions where the vertical vorticity is positive (cyclonic). The third term on the right-hand side of (3.10) represents a contribution due to the horizontal component of $\boldsymbol{\Omega}$. It is this term that helps to balance the Coriolis forces acting on the vertical flows. This term produces high pressure centred on regions of negative northward vorticity and low pressure in regions of positive northward vorticity. The positions of these pressure contributions are shown in figure 9 for the flow field produced in the fourth case. By producing high-pressure regions to the west of the updraughts the pressure contribution due to the horizontal component of $\boldsymbol{\Omega}$ can balance the westward Coriolis force on the upward motions. This is another general result that carries over from linear theory and was first explained by Cowling (1951). For case 3 this contribution is insufficient for balancing the Coriolis force, and the fluid moves westward as it moves upward. For case 4 this contribution is much stronger, and the pressure gradient nearly balances the Coriolis force so that the fluid moves nearly vertically upward.

For plane parallel layers both the linear calculations (Flasar & Gierasch 1978; Hathaway *et al.* 1979, 1980) and our present nonlinear calculations indicate that the upward flux of zonal momentum is always less than or equal to zero. Yet both the linear spherical-shell calculations (Gilman 1975; Busse & Cuong 1977) and Gilman's (1977) nonlinear calculations show that this flux can become positive for thick spherical shells. The source of this positive upward flux of angular momentum must

be attributed to non-local effects in thick shells. The pressure field produced by the Coriolis forces does have an eastward tilt with height as seen in figure 9. For the local analysis we do with plane parallel layers this tilt can just balance the opposite tilt in the fluid motions produced by the Coriolis forces. However, for a thick spherical shell the strength of the Coriolis force on the vertical motions diminishes with increasing latitude. This must produce a situation in which the pressure field then dominates the flow and forces upward-moving fluid to move eastward. Gilman's (1979) calculations for spherical shells of different depths indicate that this upward momentum flux occurs primarily in the equatorial region, where convective rolls aligned with the rotation axis extend across the equator from one hemisphere to the other.

In addition to the vertical fluxes of momentum a strong latitudinal flux of zonal momentum, given by $\langle uv \rangle$, is produced by the horizonal component of the rotation vector. This flux vanishes at the poles and at the equator and is directed toward the equator in between. Thus there should be a divergence of zonal momentum from the poles and a convergence at the equator. Of course we cannot determine the magnitude of the flow produced by this flux from the local analysis we do here. We can, however, predict that this flux should produce rapidly rotating equators like those observed on the sun and on Jupiter and Saturn. The spherical-shell studies of Busse (1970*b*), Gilman (1975) and Busse & Cuong (1977) also suggest that this flux is of major importance in producing large-scale flows in rotating systems. Gilman's (1977) nonlinear calculations for rotating spherical shells show that for rapidly rotating cases this latitudinal flux overpowers the vertical flux in producing differential rotation, but under those conditions the Coriolis forces are also important.

4. Conclusions

We find that rotation produces striking changes in the convective motions. The vertical component of the rotation vector tends to inhibit the motions and produce much smaller convection cells, with substantial turning of the fluid flow. The horizontal component of the rotation vector introduces a preference for cells elongated along the direction of the rotation axis and produces dynamical changes, which drive mean flows and horizontal heat and momentum fluxes.

Both components of the rotation vector influence the heat transport. The vertical heat flux is smaller in the high latitudes, where the vertical component of the rotation vector is largest. The mean flows produced by the horizontal component of the rotation vector carry an equatorward heat flux. This latitudinal heat flux should heat the equatorial regions and produce a temperature difference between the equator and the poles. This latitudinal temperature gradient may very well alter the mean flows, but the periodic boundary conditions in our model prohibit the formation of any horizontal temperature gradients.

The heat transports also depend upon the magnitude of the rotation rate, but in a complicated manner. When the rotation vector is vertical the vertical heat flux can increase slightly and then decrease as the rotation rate is increased. Rossby (1969) found this effect in his laboratory experiments with water. Somerville (1971) and Somerville & Lipps (1973) showed that this non-monotonic dependence of the heat flux upon the rotation rate is due to variations in the horizontal structure of the convection cells. In our numerical experiments with the tilted rotation vector we also find an increase in the heat flux with increasing rotation rate. Here, however, this increase is due to changes in the vertical structure of the convection cells. For moderate rotation rates the fluid moves upwards and towards the west along a tilted

trajectory. For more rapid rotation rates the pressure field balances the Coriolis forces and produces trajectories that are nearly vertical and more efficient at transporting heat across the layer. The horizontal heat flux also has a non-monotonic dependence upon the rotation rate. The mean flows that carry this heat flux first increase as the rotation rate increases and then decrease with further increases as the pressure field balances the Coriolis forces.

The horizontal component of the rotation vector is responsible for the fluxes of angular momentum within the system. Downward motions are turned to the east, thereby producing a downward flux of angular momentum. Although this flux decreases when the pressure field balances the Coriolis forces it never becomes an upward flux for these plane parallel layers. Yet the calculations of Gilman (1975, 1977) and Busse & Cuong (1977) shows this flux being directed upwards in the equatorial regions of spherical shells. This suggests that our local plane parallel analysis should only be applied poleward of those latitudes. We note that observations of solar p-mode oscillations (Deubner, Ulrich & Rhodes 1979), the rotation rate of supergranules (Duvall 1980), and solar dynamo activity all indicate that the solar rotation rate increases inward, at least across the shallow surface layers where our plane parallel analysis is most appropriate.

The equatorward flux of angular momentum is present in both the plane parallel and spherical geometries. The horizontal component of the rotation vector favours convection cells that are elongated in a north–south direction. In the absence of the vertical component of the rotation vector such cells produce horizontal flows that are directed to the east and to the west. The vertical component of Ω turns these flows to the right so that eastward flows are also equatorward flows and westward flows are also poleward flows. This equatorward flux of angular momentum produces faster rotation rates in the equatorial regions, as is observed on the Sun and on the giant planets.

Although the four cases we study here provide a meagre sampling of the parameters and are dominated by dissipation, they do demonstrate a number of important effects due to the tilted rotation vector. These effects may be instrumental in understanding the circulations that arise in a variety of geophysical and astrophysical systems. A spherical-shell model may be required to answer some questions about the final distribution of heat and angular momentum within such systems. However, our plane parallel model allows us to examine the detailed structure of the convective motions while producing most of the heat and momentum fluxes found to be important in the full spherical geometry.

We wish to express our sincere gratitude to Tzvi Gal-Chen for his assistance in producing the computer code and for his scientific advice on the early results. We would also like to thank Vic Borgogno, Marvin Brown, Mike Moxey, and the entire staff at the Research Data Support System of the Research Systems Facility at the National Center for Atmospheric Research (NCAR) for their assistance in producing the computer movie of our calculations. Andy Stanger and Rainer Illing of the High Altitude Observatory at NCAR also provided valuable information on the data format and production of the ciné film. Scientific discussions with Peter Gilman, also at the High Altitude Observatory, were very helpful in understanding the non-local influences on the momentum fluxes. Jackson Herring read the final manuscript and contributed helpful comments about the presentation. Finally we would like to thank the Advanced Study Program, the High Altitude Observatory, and the Scientific Computing Facility at NCAR for their support of this research.

The National Center for Atmospheric Research is sponsored by the National Science Foundation.

REFERENCES

BAKER, L. & SPIEGEL, E. A. 1975 Modal analysis of convection in a rotating fluid. *J. Atmos. Sci.* **32**, 1909.

BUSSE, F. H. 1970*a* Thermal instabilities in rapidly rotating systems. *J. Fluid Mech.* **11**, 441.

BUSSE, F. H. 1970*b* Differential rotation in stellar convection zones. *Astrophys. J.* **159**, 629.

BUSSE, F. H. & CUONG, P. G. 1977 Convection in rapidly rotating spherical fluid shells. *Geophys. Astrophys. Fluid Dyn.* **8**, 17.

BUSSE, F. H. & HEIKES, K. E. 1980 Convection in a rotating layer: a simple case of turbulence. *Science* **208**, 173.

CHANDRASEKHAR, S. 1961 *Hydrodynamic and Hydromagnetic Stability.* Oxford University Press.

CHORIN, A. J. 1968 Numerical solution of the Navier–Stokes equations. *Math. Comput.* **22**, 745.

CLEVER, R. M. & BUSSE, F. H. 1979 Nonlinear properties of convection rolls in a horizontal layer rotating about a vertical axis. *J. Fluid Mech.* **94**, 609.

COWLING, T. G. 1951 The condition for turbulence in rotating stars. *Astrophys. J.* **114**, 272.

DEUBNER, F.-L., ULRICH, R. K. & RHODES, E. J. 1979 Solar p-mode oscillations as a tracer of radial differential rotation. *Astron. Astrophys.* **72**, 177.

DUVALL, T. L. 1980 The equatorial rotation rate of the supergranulation cells. *Solar Phys.* **66**, 213.

FLASAR, F. M. & GIERASCH, P. J. 1978 Turbulent convection within rapidly rotating superadiabatic fluids with horizontal temperature gradients. *Geophys. Astrophys. Fluid Dyn.* **10**, 175.

GILMAN, P. A. 1975 Linear simulations of Boussinesq convection in a deep rotating spherical shell. *J. Atmos. Sci.* **32**, 1331.

GILMAN, P. A. 1977 Nonlinear dynamics of Boussinesq convection in a deep rotating spherical shell. *Geophys. Astrophys. Fluid Dyn.* **8**, 93.

GILMAN, P. A. 1979 Model calculations concerning rotation at high solar latitudes and the depth of the solar convection zone. *Astrophys. J.* **231**, 284.

HATHAWAY, D. H. 1982 Nonlinear simulations of solar rotation effects in supergranules. *Solar Phys.* **77**, 341.

HATHAWAY, D. H., GILMAN, P. A. & TOOMRE, J. 1979 Convective instability when the temperature gradient and rotation vector are oblique to gravity. I. Fluids without diffusion. *Geophys. Astrophys. Fluid Dyn.* **13**, 289.

HATHAWAY, D. H., TOOMRE, J. & GILMAN, P. A. 1980 Convective instability when the temperature gradient and rotation vector are oblique to gravity. II. Real fluids with effects of diffusion. *Geophys. Astrophys. Fluid Dyn.* **15**, 7.

HEARD, W. B. 1972 Thermal convection in a rotating, thin spherical annulus of fluid. Ph.D. Thesis, Yale University.

HEARD, W. B. & VERONIS, G. 1971 Asymptotic treatment of the stability of a rotating layer of fluid with rigid boundaries. *Geophys. Fluid Dyn.* **2**, 299.

KOSCHMIEDER, E. L. 1967 On convection in a uniformly heated rotating frame. *Beitr. Phys. Atmos.* **40**, 216.

KRISHNAMURTI, R. 1971 On the transition to turbulent convection. *8th Symp. Naval Hydrodyn. Rep.* ARC-179, p. 289. Office of Naval Res., Washington D.C.

KUPPERS, G. 1970 The stability of steady finite amplitude convection in a rotating layer. *Phys. Lett.* **32**, 7.

KUPPERS, G. & LORTZ, D. 1969 Transition from laminar convection to thermal turbulence in a rotating fluid layer. *J. Fluid Mech.* **35**, 609.

LORENZ, E. N. 1967 *The Nature and Theory of the General Circulation of the Atmosphere.* World Met. Orgn, Geneva.

ROBERTS, P. H. 1968 On the thermal instability of a rotating fluid sphere containing heat sources. *Phil. Trans. R. Soc. Lond.* A **263**, 93.

ROSSBY, H. T. 1969 A study of Bénard convection with and without rotation. *J. Fluid Mech.* **36**, 309.

SOMERVILLE, R. C. J. 1971 Bénard convection in a rotating fluid. *Geophys. Fluid Dyn.* **2**, 247.

SOMERVILLE, R. C. J. & GAL-CHEN, T. 1979 Numerical simulation of convection with mean vertical motion. *J. Atmos. Sci.* **36**, 805.

SOMERVILLE, R. C. J. & LIPPS, F. B. 1973 A numerical study in three space dimensions of Bénard convection in a rotating fluid. *J. Atmos. Sci.* **30**, 590.

VAN DER BORGHT, R. & MURPHY, J. O. 1973 The effect of rotation on nonlinear thermal convection. *Austral. J. Phys.* **26**, 341.

VERONIS, G. 1959 Cellular convection with finite amplitude in a rotating fluid. *J. Fluid Mech.* **5**, 401.

VERONIS, G. 1968 Large-amplitude Bénard convection in a rotating fluid. *J. Fluid Mech.* **31**, 113.

WEISS, N. O. 1964 Convection in the presence of constraints. *Phil. Trans. R. Soc. Lond.* A **256**, 99.

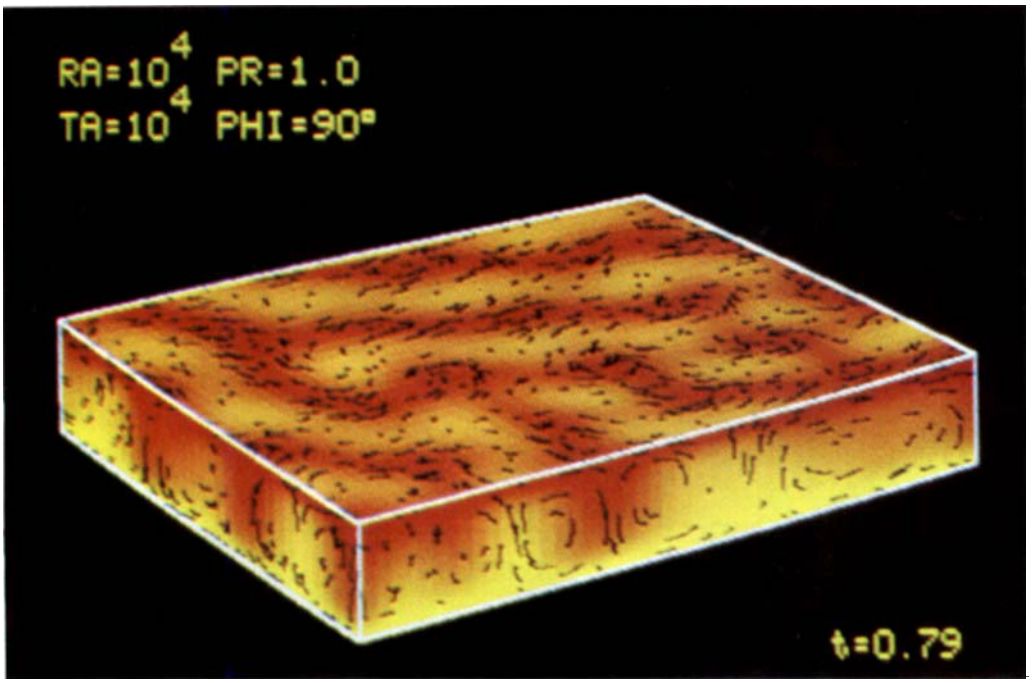

FIGURE 4. Perspective view of the velocity and temperature field for case 1. Colour is used to represent temperature, with yellow being the hottest and red the coldest. Particle trajectories are shown for particles that are confined to each of the three surfaces shown. Overturning motions are seen in the two vertical surfaces with warm updrafts and cool downdrafts. The horizontal upper surface shows the outflows from the updrafts and the convergence in the downdrafts.

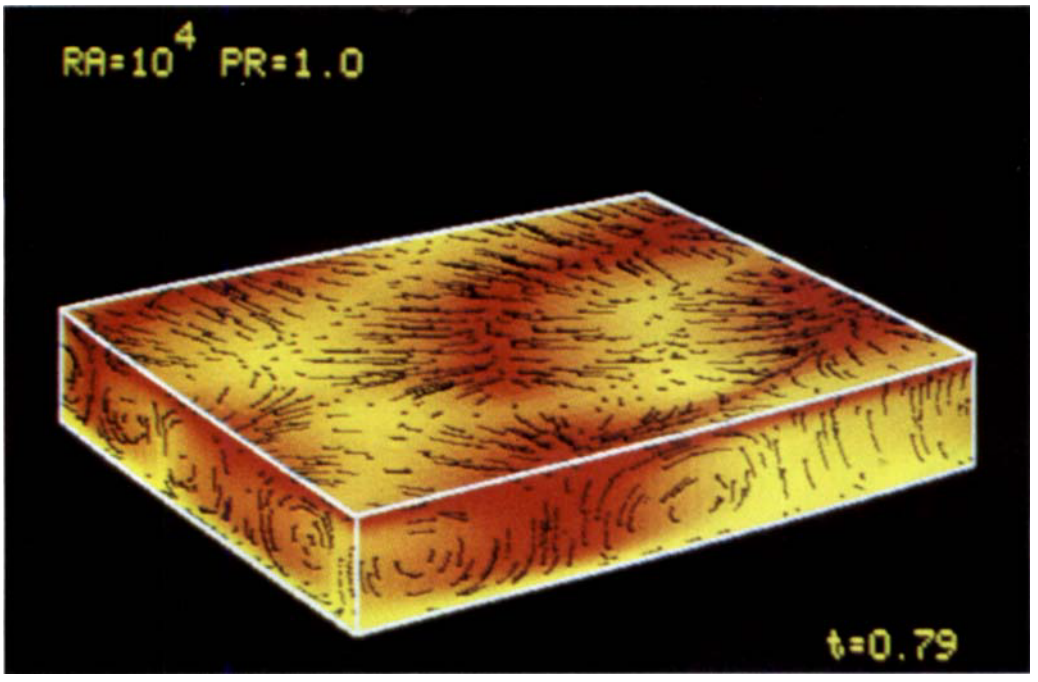

FIGURE 5. Velocity and temperature field for case 2. Here the cells are small compared with the depth of the layer. Cyclones are formed in the cool downdrafts on the upper surface while anticyclones are formed in the updrafts.

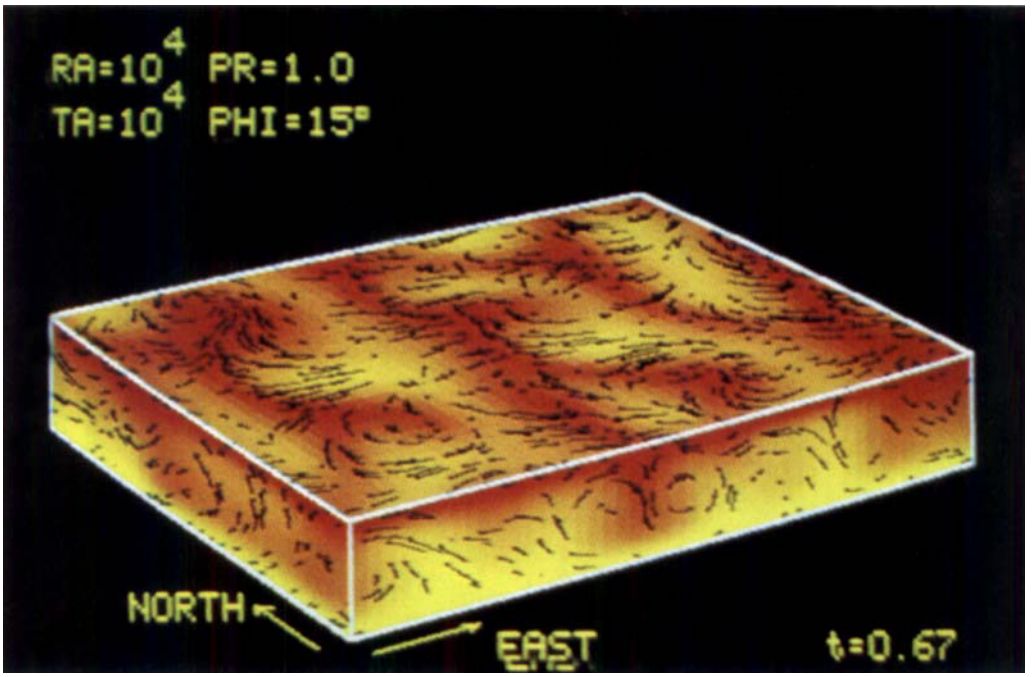

FIGURE 6. Velocity and temperature field for case 3. The upper surface shows the elongated cells oriented north to south as well as a predominately westward flow in the warm updrafts. The southern vertical surface also shows that the upward motions are correlated with westward motions owing to the influence of the tilted rotation vector.

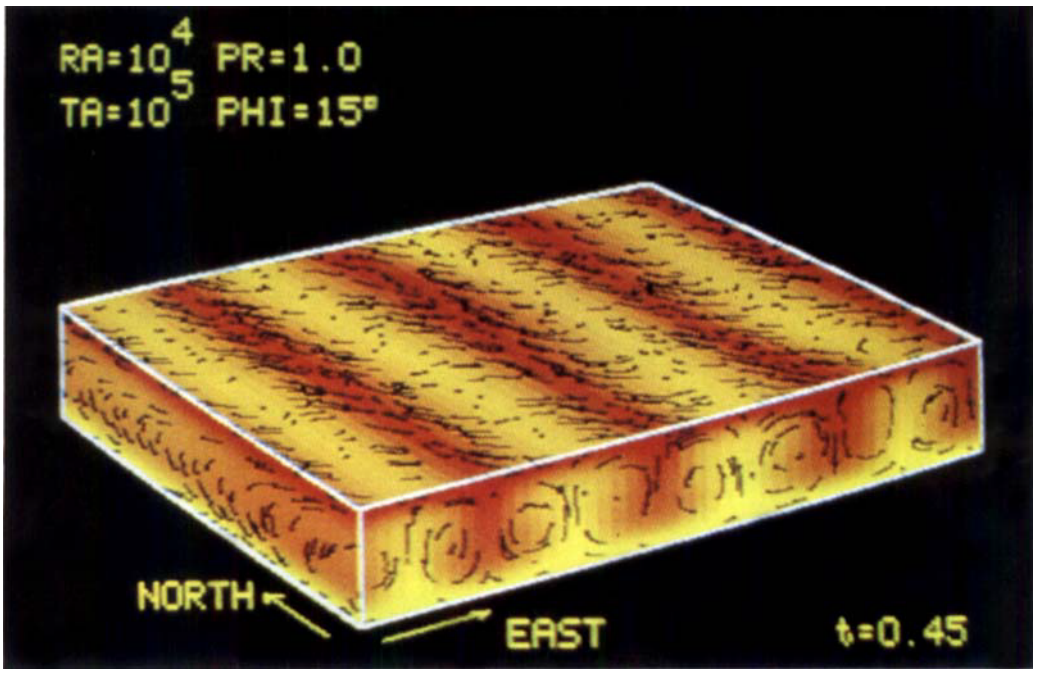

FIGURE 7. Velocity and temperature field for case 4. The tilted rotation vector constrains the flow rigidly to a series of north–south rolls. The vertical flows have only a slight westward tilt owing to the nearly perfect balance between the Coriolis force and pressure gradients. The horizontal flows are strongly correlated with eastward-moving fluid also moving towards the equator.